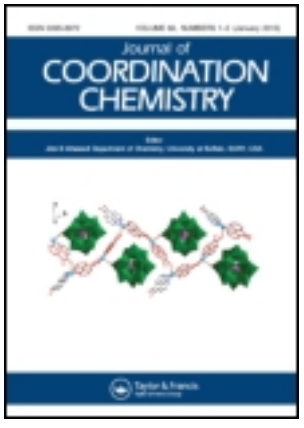

Journal of Coordination Chemistry
Publication details, including instructions for authors and subscription information:
http://www.tandfonline.com/loi/gcoo20

Two 2-D layered coordination polymers based on 5-aminoisophthalate and 1,10-phenanthroline

Jing-Jing Wang [a], Qi-Long Bao [a] & Jin-Xi Chen [a]
[a] School of Chemistry and Chemical Engineering, Southeast University, Nanjing, P.R. China
Published online: 04 Jul 2013.

To cite this article: Jing-Jing Wang, Qi-Long Bao & Jin-Xi Chen (2013) Two 2-D layered coordination polymers based on 5-aminoisophthalate and 1,10-phenanthroline, Journal of Coordination Chemistry, 66:14, 2578-2586, DOI: 10.1080/00958972.2013.813939

To link to this article: http://dx.doi.org/10.1080/00958972.2013.813939

Journal of Coordination Chemistry, 2013
Vol. 66, No. 14, 2578–2586, http://dx.doi.org/10.1080/00958972.2013.813939

Two 2-D layered coordination polymers based on 5-aminoisophthalate and 1,10-phenanthroline

JING-JING WANG, QI-LONG BAO and JIN-XI CHEN*

School of Chemistry and Chemical Engineering, Southeast University, Nanjing, P.R. China

(*Received 1 November 2012; in final form 23 April 2013*)

Two new compounds, $[Zn(aip)(phen)]_n$ (**1**) and $[Mn(aip)(phen)]_n$ (**2**) (H_2aip = 5-aminoisophthalic acid, phen = 1,10-phenanthroline), have been synthesized by solvothermal methods and structurally characterized. X-ray diffraction analyses indicate that **1** and **2** have a 2-D layer structure, with aip^{2-} adopting two coordination motifs. The coordination configuration of the metal plays a crucial role in formation of different topological structures. Thermogravimetric analyses of **1** and **2** show considerable thermal stability. The fluorescence of **1** and **2** in the solid state has also been investigated.

Keywords: Zinc; Manganese; 5-Aminoisophthalic acid; Fluorescence

1. Introduction

Synthesis of coordination polymers (CPs) stems from intriguing architectures and topologies [1–5] and also from potential applications as functional materials, including luminescence [6], gas absorption and separation [7], catalysis [8], and magnetism [9]. One of the most effective approaches to obtain CPs is hydro(solvo)thermal assembly by incorporating appropriate metal ions (connectors) with multifunctional bridging ligands (linkers) [10]. However, construction of CPs can be influenced by several factors, such as the nature of the metal ions, solvent, and temperature [10, 11]. Among those factors, the coordination configuration of metal ions usually governs topological structures. Through elaborate choice of organic ligands and metals, a multitude of CPs with different topological architectures have been reported, and several of them (such as ZIF-8, HKUST-1, and MIL-53) are available commercially [12, 13]. Of the reported CPs, many are based on polyfunctional organic ligands containing both carboxylate and amino groups, such as 2-aminoterephthalic acid [14], 3-aminobenzoic acid [15], and 5-aminoisophthalic acid [16].

5-Aminoisophthalic acid (H_2aip) has been chosen as ligand for construction of CPs based on two considerations. One, H_2aip can adopt various coordination modes and can be an outstanding candidate for construction of multiple structural moieties due to its bridging fragments. Two, limited effort has been made so far towards investigation of CPs constructed from H_2aip [17], and further work is needed. Moreover, the introduction of N-containing ligands such as 1,10-phen or 4,4′-bipy (4,4′-bipy = 4,4′-bipyridine) may

*Corresponding author. Email: chenjinxi@seu.edu.cn

induce new topologies. A 1,10-phen or 4,4′-bipy may provide potential π–π stacking interactions and supramolecular recognition sites for hydrogen bonding [18–20]. Herein, we report two 2-D CPs, $[Zn(aip)(phen)]_n$ (**1**) and $[Mn(aip)(phen)]_n$ (**2**), based on H_2aip and 1,10-phen. The fluorescence properties of **1** and **2** in the solid state are also discussed.

2. Experimental

2.1. *Materials and methods*

All reagents and solvents were commercially available and used directly without purification. C, H, and N elemental analyses were performed on a Perkin-Elmer 240C analyzer. Infrared (IR) spectra were recorded as KBr pellets from 4000 to 400 cm^{-1} on a Nicolet Avatar 360 FTIR spectrometer. Thermogravimetric analyses were obtained on a TA Q20 USA instrument with a heating rate of 10 °C min^{-1} from 50 to 800 °C under nitrogen. The fluorescence properties were measured on a FluoroMax 4 spectrofluorometer.

2.2. *Synthesis*

2.2.1. $[Zn(aip)(phen)]_n$ (1). A mixture of H_2aip (0.5 mM, 0.09057 g), 1,10-phen (0.5 mM, 0.0901 g), and $Zn(NO_3)_2{\cdot}6H_2O$ (0.5 mM, 0.1487 g) was added to 10 mL DMF/H_2O (V/V = 1) in a 25 mL Teflon-lined stainless steel vessel and stirred at ambient temperature for five minutes. The vessel was sealed and heated at 120 °C for three days. After cooling, colorless sheet-like crystals (0.0846 g, 40% based on Zn) were obtained by filtration and washed with H_2O and EtOH several times. Anal. Calcd for $C_{20}H_{13}N_3O_4Zn$ (%): C, 56.51; H, 3.06; N, 9.89. Found: C, 57.31; H, 3.15; N, 9.93. IR (KBr, cm^{-1}): 3265(w), 1620(s), 1580(w), 1556(s), 1517(s), 1426(w), 1395(w), 1351(vs), 1314(s), 1144(vw), 1087(s), 959(w), 851(s), 778(vs), 727(s).

2.2.2. $[Mn(aip)(phen)]_n$ (2). A mixture of H_2aip (0.25 mM, 0.0453 g), 1,10-phen (0.25 mM, 0.0451 g) and $Mn(OAc)_2{\cdot}4H_2O$ (0.25 mM, 0.0617 g) was added to 10 mL DMF/EtOH (V/V = 1) in a 25 mL Teflon-lined stainless steel vessel and stirred at ambient temperature for ten minutes. The vessel was sealed and heated at 150 °C for three days. After cooling, brown, block-shaped crystals (0.0495 g, 48% based on Mn) were obtained by filtration and washed with H_2O and EtOH several times. Anal. Calcd for $C_{20}H_{13}MnN_3O_4$ (%): C, 57.93; H, 3.14; N, 10.14. Found: C, 58.12; H, 3.20; N, 10.25. IR (KBr, cm^{-1}): 3446(s), 3349(s), 1572(s), 1544(s), 1515(w), 1468(s), 1423(s), 1376(s), 1141 (vw), 1101(w), 1002(w), 849(s), 782(s), 723(s), 638(w), 575(w), 433(w).

2.3. *X-ray crystallography*

Data were collected at 293 K using a Bruker Smart Apex II diffractometer with graphite monochromated Mo Kα (λ = 0.71073 Å) radiation in ω scan mode. These structures were solved by direct methods and refined with Fourier techniques. Anisotropic thermal parameters were used for all non-hydrogen atoms in the full matrix least squares

Table 1. Crystal data and structure refinement parameters for **1** and **2**.

	1	**2**
Empirical formula	$C_{20}H_{13}N_3O_4Zn$	$C_{20}H_{13}MnN_3O_4$
Formula weight	424.72	414.27
Crystal size (mm)	0.25 × 0.2 × 0.2	0.25 × 0.25 × 0.3
Temperature (K)	293(2)	293(2)
Wavelength (Å)	0.71073	0.71073
Crystal system	Triclinic	Monoclinic
Space group	*P-1*	*P2(1)/n*
a (Å)	8.2982(17)	11.231(2)
b (Å)	8.4293(17)	12.599(3)
c (Å)	13.305(3)	13.981(3)
α (°)	75.08(3)	90
β (°)	84.37(3)	99.25(3)
γ (°)	78.89(3)	90
U (Å^3)	881.3(3)	1952.6(7)
Z	2	4
D (calcd) (Mg m^{-3})	1.601	1.409
μ (mm^{-1})	1.427	0.706
F (0000)	432	844
θ range for data collection (°)	3.03–25.01	3.01–25.01
Limiting indices	$-9 \leqslant h \leqslant 9$, $-10 \leqslant k \leqslant 10$, $-15 \leqslant l \leqslant 15$	$-13 \leqslant h \leqslant 13$, $-14 \leqslant k \leqslant 14$, $-16 \leqslant l \leqslant 16$
Reflections collected/unique	7192/3042 [*R*(int) = 0.1509]	16,563/3434 [*R*(int) = 0.0674]
Completeness to theta%	98.2	99.8
Refinement method	Full-matrix least-squares on F^2	Full-matrix least-squares on F^2
Data/restraints/parameters	3042/4/187	3434/0/261
Goodness-of-fit on F^2	0.906	1.135
Final *R* indices [I > 2*σ* (I)]	$R_1{}^a = 0.0576$, $wR_2{}^b = 0.1101$	$R_1{}^a = 0.0618$, $wR_2{}^b = 0.2012$
R indices (all data)	$R_1{}^a = 0.1068$, $wR_2{}^b = 0.1238$	$R_1{}^a = 0.0760$, $wR_2{}^b = 0.2126$
Largest diff. peak and hole (e.A^{-3})	0.787 and −0.801	1.780 and −0.367

$^a R = \Sigma||F_0| - |F_c||/\Sigma|F_0|$. $^b wR\ (F^2) = [\Sigma w(F_o^2 - F_c^2)^2/\Sigma w(F_o^2)^2]^{1/2}$. $w = 1/[\sigma^2(P)^2 + 0.00^*P]$; with $P = (\text{Max}\ (F_o^2, 0) + 2\ F_c^2)/3$ for **1**. $w = 1/[\sigma^2(F_o^2) + (0.1285P)^2 + 1.97^*P]$, where $P = (\text{Max}\ (F_o^2, 0) + 2\ F_c^2)/3$ for **2**.

refinements based on F^2. All calculations were performed with SHELXL-97 [21]. The crystallographic data and structure refinement parameters for **1** and **2** are given in table 1. Selected bond distances and angles for **1** and **2** are listed in table 2.

3. Results and discussion

3.1. *Structure descriptions of 1 and 2*

The single-crystal X-ray diffraction analysis revealed that **1** has a 2-D layer structure and crystallized in the triclinic space group (*P-1*) with one Zn^{2+}, one aip^{2-}, and one 1,10-phen in the asymmetric unit. As shown in figure 1(a), Zn^{2+} displays a distorted trigonal-bipyramidal geometry and is surrounded by two carboxylic oxygens [Zn(1)–O(1) = 2.140(3) Å and Zn(1)–O(2A) = 2.121(3) Å] from two distinct aip^{2-} and three nitrogens [Zn(1)–N(1) = 2.260(5) Å, Zn(1)–N(2) = 2.167(4) Å and Zn(1)–N(3B) = 2.257(5) Å] from one 1,10-phen and one aip^{2-}. N(1) and N(3B) are axial and the equatorial plane is occupied by O(1), O(2A), and N(2). The O(1)–Zn(1)–O(2A), O(2A)–Zn(1)–N(2), and N(2)–Zn(1)–O(1) angles are 100.62°, 112.03°, and 139.79°; the sum is 352.44°. The angles between the axial atoms and the equatorial atoms range from 76.38° to 104.27°. The bond distances and angles all

Table 2. Selected bond lengths (Å) and angles (°) for **1** and **2**.

Compound **1**			
Zn(1)–O(2)^{A}	2.121(3)	Zn(1)–N(1)	2.260(5)
Zn(1)–O(1)	2.140(3)	Zn(1)–N(3)^{B}	2.257(5)
Zn(1)–N(2)	2.167(4)		
O(2)^{A}–Zn(1)–O(1)	100.62(12)	N(2)–Zn(1)–N(1)	76.38(17)
O(2)^{A}–Zn(1)–N(2)	112.03(14)	N(3)^{B}–Zn(1)–N(1)	172.35(12)
O(1)–Zn(1)–N(2)	139.79(13)	O(2)^{A}–Zn(1)–O(3)	157.07(12)
O(2)^{A}–Zn(1)–N(3)^{B}	98.63(14)	O(1)–Zn(1)–O(3)	56.91(11)
O(1)–Zn(1)–N(3)^{B}	92.91(14)	N(2)–Zn(1)–O(3)	87.24(12)
N(2)–Zn(1)–N(3)^{B}	104.27(18)	N(3)^{B}–Zn(1)–O(3)	87.91(13)
O(2)^{A}–Zn(1)–N(1)	88.05(15)	N(1)–Zn(1)–O(3)	84.50(14)
O(1)–Zn(1)–N(1)	82.13(14)		
Compound **2**			
Mn(1)–O(1)	2.099(3)	Mn(1)–N(2)	2.249(4)
Mn(1)–O(2)^{A}	2.143(3)	Mn(1)–O(3)^{B}	2.294(3)
Mn(1)–O(4)^{B}	2.229(3)	Mn(1)–N(3)	2.314(4)
O(1)–Mn(1)–O(2)^{A}	99.93(13)	O(2)^{A}–Mn(1)–O(3)^{B}	89.50(12)
O(1)–Mn(1)–O(4)^{B}	99.43(13)	O(4)^{B}–Mn(1)–O(3)^{B}	58.11(11)
O(2)^{A}–Mn(1)–O(4)^{B}	95.29(13)	N(2)–Mn(1)–O(3)^{B}	95.60(13)
O(1)–Mn(1)–N(2)	103.54(14)	O(1)–Mn(1)–N(3)	89.61(14)
O(2)^{A}–Mn(1)–N(2)	100.57(14)	O(2)^{A}–Mn(1)–N(3)	169.55(13)
O(4)^{B}–Mn(1)–N(2)	149.22(14)	O(4)^{B}–Mn(1)–N(3)	87.26(15)
O(1)–Mn(1)–O(3)^{B}	156.59(13)	N(2)–Mn(1)–N(3)	72.81(15)
O(3)^{B}–Mn(1)–N(3)	83.24(14)		

Symmetry transformations used to generate equivalent atoms: $^{A}x-1, y+1, z$, $^{B}x-1, y, z$ for **1**; $^{A}-x+2, -y+2, -z$, $^{B}x-1/2, -y+3/2, z-1/2$ for **2**.

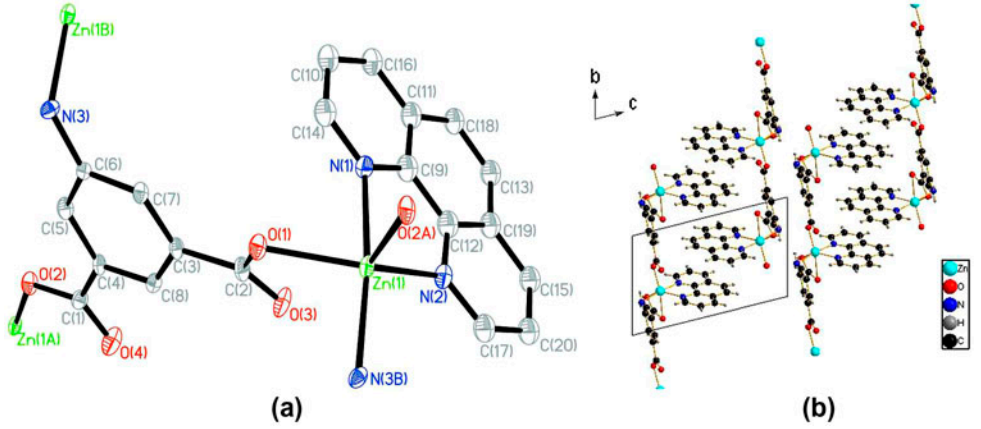

Figure 1. (a) Coordination environment of Zn in **1** with 30% probability thermal ellipsoids; symmetry transformation: *A*, *x* − *1*, *y* + *1*, *z*; *B*, *x* − *1*, *y*, *z*; all hydrogens are omitted for clarity. (b) View of 2-D layer network along the *a* axis.

lie in the normal range for reported Zn complexes [22–25]. In **1**, the carboxylate of aip^{2-} is monodentate bridging and the amino of aip^{2-} ligates Zn^{2+}. Each aip^{2-} bridges three metal centers and extends the structure into a 2-D layer. The 1,10-phen ligands are located on one side of the layer (figure 1(b)) and there are π–π interactions between them. The

face to face distance of parallel benzene rings (C9, C11, C18, C13, C19, and C12) of 1,10-phen in neighboring layers is 3.890 Å. Every pair of layers are interconnected by N–H···O hydrogen bonds (table 3) between the amino and the carboxylate of different aip^{2-}, packing into a 2-D network (figure S1).

X-ray diffraction analysis revealed that **2** crystallized in the monoclinic space group $P2(1)/n$ and consists of a 2-D layer structure. In the asymmetric unit of **2**, there are one unique Mn^{2+}, one aip^{2-} and one 1,10-phen. As shown in figure 2(a), Mn^{2+} is six-coordinate in a distorted octahedral geometry, consisting of two nitrogens [Mn(1)–N(2) = 2.249 (4) Å and Mn(1)–N(3) = 2.314(4) Å] from one 1,10-phen and four oxygens [Mn(1)–O(1) = 2.099(3) Å, Mn(1)–O(2A) = 2.143(3) Å, Mn(1)–O(3B) = 2.294(3) Å and Mn(1)–O(4B) = 2.229(3) Å] from three different aip^{2-}. The distortion from octahedral geometry can mainly be attributed to the acute chelate angles from phen (N(3–Mn(1)–N(2) = 72.81°) and the chelated carboxylate (O(4B–Mn(1)–O(3B) = 58.11°). N(3) and O(2A) are axial, and the equatorial plane consists of O(1), O(4B), O(3B), and N(2). Bond distances and angles lie in the normal range of reported Mn complexes [26–28]. In **2**, one of the two carboxylates adopts a chelating coordination mode while the other bridges two Mn, forming an eight-membered $Mn_2C_2O_4$ ring. In the ring, O1–Mn–O2A angle is 99.945° and the distance of Mn···Mn is 4.4465 Å, both of which are close to corresponding values for $[Mn(pbc)_2]_n$ (pbc = 3-pyridyl-3-ylbenzoic acid) [29]. The chelating carboxylate has longer Mn–O bonds than the monodentate bridging one (2.294(3) and 2.229(3) Å > 2.099(3) and 2.143(3) Å). Each aip^{2-} links three Mn^{2+} cations through four carboxylic oxygens to form an infinite 2-D layer structure in which there are N–H···O hydrogen bond interactions between adjacent aip^{2-} (figure S2, table 3). The 1,10-phen ligands are located on both sides of the layer. The dihedral angle is 82.77° between 1,10-phen and the phenyl ring of aip^{2-}. The layers are packed along the b axis (figure 2(b)).

The aip^{2-} adopts two coordination motifs. The coordination configuration of the metal ion plays a crucial role in construction of CPs. The difference between **1** and **2** is the location of phen and the coordination of aip^{2-}, caused by the different metal centers with different coordination numbers and geometries. Both **1** and **2** have some structural similarity, in that aip^{2-} links metal ions to form layered structures. In reported compounds containing similar ligands [30–32], aromatic dicarboxylic acid ligands are excellent linkers to form 2-D layer structures. In addition, $[Zn(HA)_2(2,2'\text{-bipy})]_2$ (HA = 2-hydroxy-3-naphthoate) [33] and $[Mn(C_8H_4O_5)(2,2'\text{-bipy})]\cdot H_2O$ ($C_8H_4O_5$ = 5-hydroxyisophthalate) [34] have the same geometrical configuration as **1** and **2**, respectively. The eight-membered $Mn_2C_2O_4$ ring is also present in $[Mn(C_8H_4O_5)(2,2'\text{-bipy})]\cdot H_2O$.

Table 3. Hydrogen bond lengths (Å) and angles (°) for **1** and **2**.

D–H···A	d(D–H)/Å	d(H···A)/Å	d(D···A)/Å	∠D–H···A/°
Compound **1**				
N3–H3A···O1 #1	0.86	2.37	3.056(5)	137
Compound **2**				
N1–H6···O4 #1	0.89(7)	2.09(7)	2.953(6)	163(6)
N1–H7···O1 #2	0.96(5)	2.52(5)	3.172(5)	125(4)

Symmetry codes: #1: $1-x$, $1-y$, $-z$ for **1**; #1: $3-x$, $2-y$, $1-z$, #2: $5/2-x$, $1/2+y$, $1/2-z$ for **2**.

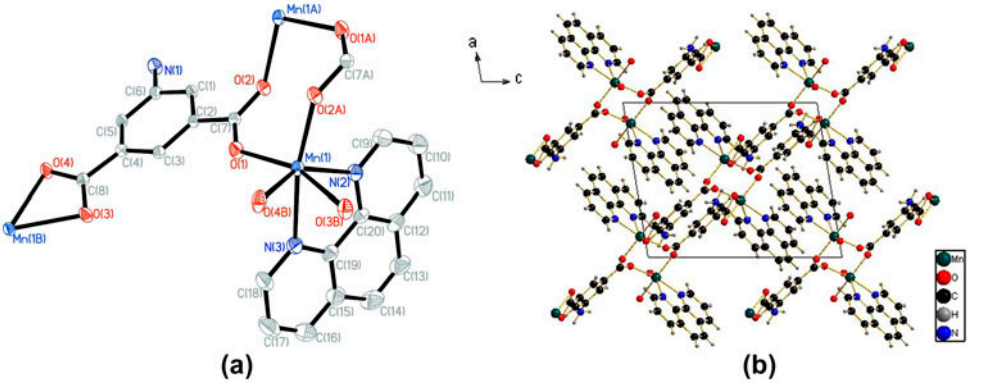

Figure 2. (a) Coordination environment of Mn in **2** with 30% probability thermal ellipsoids; symmetry transformation: *A*, $-x+2, -y+2, -z$; *B*, $x-1/2, -y+3/2, z-1/2$; all hydrogens are omitted for clarity. (b) View of 2-D layer network along the *b* axis.

3.2. *PXRD, IR spectra, and thermal properties*

Simulated and experimental PXRD patterns of **1** and **2** obtained at room temperature are shown in figure S3. Diffraction peaks of simulated and experimental patterns match well in relevant positions, indicating that the phase purities of **1** and **2** are good.

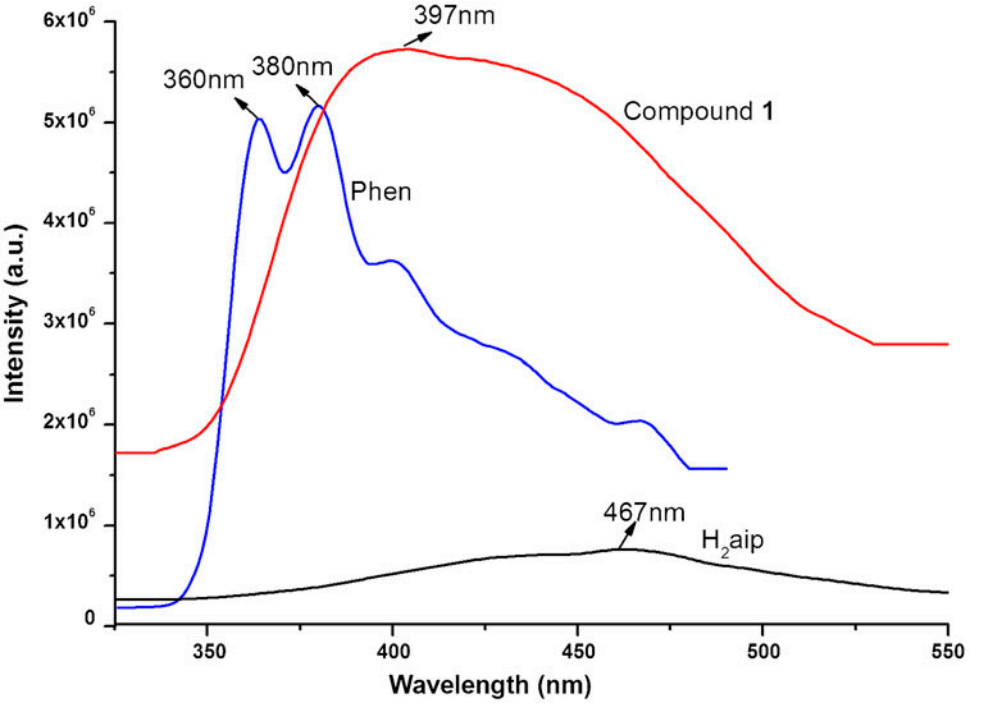

Figure 3. Solid-state fluorescent emission spectrum of **1** at room temperature.

In the IR spectrum of **1** (figure S4), characteristic bands of the dicarboxylate unit occur from 1620–1556 cm^{-1} for the asymmetric stretch and 1425–1351 cm^{-1} for the symmetric stretch. In the IR spectrum of **2** (figure S4), peaks at 3446 and 3349 cm^{-1} are due to N–H stretches, caused by formation of two hydrogen bonds between $–NH_2$ and carboxylate oxygens. The strong peaks at 1572–1544 and 1423–1376 cm^{-1} can be assigned to asymmetric and symmetric stretches of dicarboxylate, respectively. There are no characteristic vibrations for –COOH between 1680 and 1760 cm^{-1}, which indicates coordination via the carboxylate in **1** and **2**. IR results are in agreement with the results from the crystal structures.

As depicted in figure S5, **1** was stable to 380 °C. The TGA curve of **1** exhibited an initial mass loss of 40.88% between 380 and 760 °C, corresponding to loss of 1,10-phen (calcd: 42.43%). Upon further heating, aip^{2-} gradually decomposed, leading to collapse of the polymeric network. Compound **2** is stable to 250 °C and, upon further heating, suffers a two stage weight loss pattern similar to that for **1**.

3.3. *Fluorescent properties*

The d^{10} MOFs have been widely investigated as excellent candidates for potential photoluminescent materials. The solid state fluorescence spectrum of free phen displayed two strong emission maxima at 360 and 380 nm with excitation at 218 nm, while a stronger fluorescent emission band was observed at 397 nm for **1** upon excitation at 300 nm, as shown in figure 3. Compared with free phen, a red-shift of emission occurred in **1**.

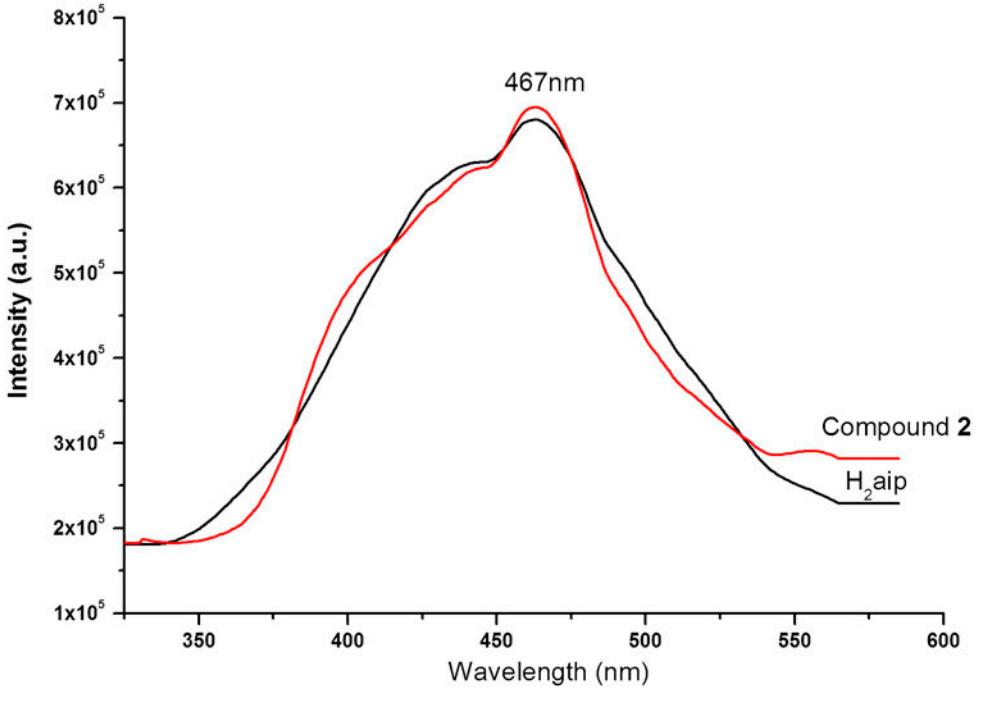

Figure 4. Solid-state fluorescent emission spectrum of **2** at room temperature.

This emission arises from the π^*–π of phen [35]. Fluorescent emission of H_2aip is much weaker than that for phen, thus aip^{2-} had almost no contribution to fluorescent emission of the complexes [36].

The solid state fluorescence spectrum of **2** at room temperature is depicted in figure 4. Compound **2** exhibited an intense emission at 467 nm at the excited wavelength of 300 nm. All emission spectra are similar with free H_2aip in shape and position. Compared with **1**, the emission intensity of **2** was reduced due to quenching by the paramagnetic Mn(II) [35].

4. Conclusion

A number of complexes with isophthalic acid and N-heterocyclic ligands coordinated to metal ions have been reported [14–16, 23]. Through self-assembly of 1,10-phen with Zn (II) and Mn(II) in the presence of H_2aip, we have synthesized two new complexes, $[Zn(aip)(phen)]_n$ (**1**) and $[Mn(aip)(phen)]_n$ (**2**). In the 2-D layer compounds **1** and **2**, aip^{2-} possesses two types of coordination modes. The coordination configuration of metal ion plays a critical role in formation of the resulting topological structures. The change of metal ion influences coordination environment of the metal centers and the conformation of aip^{2-}, and thus influences the detailed architecture of the CPs. Furthermore, the thermal and luminescent properties of **1** and **2** have been studied.

Supplementary material

Figures of the H-bonding interactions, experimental and simulated PXRD patterns, IR spectra, and TGA curves for **1** and **2**. CCDC 908382 and 908383 contain the supplementary crystallographic data for **1** and **2**. These data can be obtained free of charge from the Cambridge Crystallographic Data Center, CCDC, 12 Union Road, Cambridge, CB2 1EZ, UK [Tel: +44 (0)1223 762906; E-mail: deposit@ccdc.cam.ac.uk; http://www.ccdc.cam.ac.uk/services/structure_deposit/].

Acknowledgment

We gratefully acknowledge the financial support by the Natural Science Foundation of Jiangsu Province (Project No. BK2009262).

References

[1] Y. Fu, J. Su, S.H. Yang, G.B. Li, F.H. Liao, M. Xiong, J.H. Lin. *Inorg. Chim. Acta*, **363**, 645 (2010).
[2] T. Loiseau, C. Serre, C. Huguenard, G. Fink, F. Taulelle, M. Henry. *Chem. Eur. J.*, **10**, 1373 (2004).
[3] C. Volkringer, T. Loiseau, T. Devic, G. Férey, D. Popov, M. Burghammer, C. Riekel. *CrystEngCommun*, **12**, 3225 (2010).
[4] L.P. Wang, T.Y. Song, C. Li, J. Xia, S.Y. Wang, L. Wang, J.N. Xu. *J. Solid State Chem.*, **190**, 208 (2012).
[5] F.W. Zhang, Z.F. Li, T.Z. Ge, H.C. Yao, G. Li, H.J. Lu, Y.Y. Zhu. *Inorg. Chem.*, **49**, 3776 (2010).
[6] Y. Cui, Y. Yue, G. Qian, B. Chen. *Chem. Rev.*, **112**, 1126 (2012).
[7] (a) J.R. Li, R.J. Kuppler, H.C. Zhou. *Chem. Soc. Rev.*, **38**, 1477 (2009); (b) J.R. Li, Y. Ma, M.C. McCarthy, J. Sculleya, J. Yu, H.K. Jeong, P.B. Balbuena, H.C. Zhou. *Coord. Chem. Rev.*, **255**, 1791 (2011).
[8] (a) L. Ma, C. Abney, W. Lin. *Chem. Soc. Rev.*, **38**, 1248 (2009); (b) M. Yoon, R. Srirambalaji, K. Kim. *Chem. Rev.*, **112**, 1196 (2012).

[9] Z.B. Han, J.W. Ji, H.Y. An, W. Zhang, G.X. Han, G.X. Zhang, L.G. Yang. *Dalton Trans.*, 9807 (2009).
[10] E. Tang, Y.-M. Dai, J. Zhang, Z.-J. Li, Y.-G. Yao, J. Zhang, X.-D. Huang. *Inorg. Chem.*, **45**, 6276 (2006).
[11] H. Wu, H.Y. Liu, J. Yang, B. Liu, J.F. Ma, Y.Y. Liu, Y.Y. Liu. *Cryst. Growth Des.*, **11**, 2317 (2011).
[12] J.X. Chen, J.J. Wang, M. Ohba. *J. Solid State Chem.*, **185**, 37 (2012).
[13] J.X. Chen, B.H. Liu. *Inorg. Chem. Commun.*, **22**, 170 (2012).
[14] (a) C.B. Liu, X.J. Zheng, Y.Y. Yang, L.P. Jin. *Inorg. Chem. Commun.*, **8**, 1045 (2005); (b) D. Zhao, Y. Xiu, X.L. Zhou, X.R. Meng. *J. Coord. Chem.*, **65**, 112 (2012); (c) X.Q. Cao, X. Zheng, M.X. Chen, X.X. Xu, T. Sun, E.B. Wang. *J. Coord. Chem.*, **65**, 754 (2012).
[15] Y.H. Wei, A.Zh. Tan, Z.L. Chen, F.P. Liang, R.X. Hu. *Chin. J. Struct. Chem.*, **25**, 343 (2006).
[16] (a) Z.W. Yan, F. Li, H.F. Zeng, S.J. Luo, T.H. Li. *J. Iran. Chem. Soc.*, **7**, 978 (2010); (b) X.L. Zhang, K. Cheng. *J. Coord. Chem.*, **65**, 3019 (2012); (c) H.W. Kuai, T.A. Okamuraz, W.Y. Sun. *J. Coord. Chem.*, **65**, 3147 (2012).
[17] H.-N. Wang, X. Meng, C. Qin, X.-L. Wang, G.-S. Yang, Z.-M. Su. *Dalton Trans*., 1047 (2012).
[18] K.-L. Zhang, N. Qiao, H.-Y. Gao, F. Zhou, M. Zhang. *Polyhedron*, **26**, 2461 (2007).
[19] M.L. Hu, D.J. Xu, D.P. Cheng. *J. Coord. Chem.*, **55**, 11 (2002).
[20] Z. Zhang, M. Pi, T. Wang, C.M. Jin. *J. Mol. Struct.*, **992**, 111 (2011).
[21] G.M. Sheldrick, *SHELXTL V5.1, Software Reference Manual*, Bruker AXS Inc., Madison, WI, USA (1997).
[22] X.M. Li, Z.T. Wang, B. Liu, Q.W. Wang, S. Zhou. *Chin. J. Struct. Chem.*, **28**, 1257 (2009).
[23] J.P. Zou, S.C. Dai, W.T. Guan, H.B. Yang, Y.F. Feng, X.B. Luo. *J. Coord. Chem.*, **65**, 2877 (2012).
[24] C.A. Tolga, Y.O. Zafer, B. Orhan. *J. Inorg. Organomet. Polym.*, **20**, 26 (2010).
[25] K.O. Kongshaug, H. Fjellvåg. *Inorg. Chem.*, **45**, 2424 (2006).
[26] Y.L. Niu, X.M. Li, B. Liu, Q.W. Wang. *Chinese. J. Struct. Chem.*, **29**, 712 (2010).
[27] A. Majumder, S. Shit, C.R. Choudhury, S.R. Batten, G. Pilet, D. Luneau, N. Daro, J. Sutter, N. Chattopadhyay. *Inorg. Chim. Acta*, **358**, 3855 (2005).
[28] K.O. Kongshaug, H. Fjellvåg. *Polyhedron*, **26**, 5113 (2007).
[29] F. Guo. *J. Coord. Chem.*, **62**, 3606 (2009).
[30] Y. Huang, B. Yan, M. Shao. *Solid State Sci.*, **10**, 90 (2008).
[31] Y. Hou, E.H. Shen, S.T. Wang, E.B. Wang, C.W. Hu. *Inorg. Chem. Commun.*, **6**, 1347 (2003).
[32] (a) C.B. Liu, J.M. Zhong, H.Y. Shu, Z.Q. Xiong. *Chin. J. Chem.*, **26**, 1511 (2010); (b) H.Y. He, Y.L. Zhou, L.G. Zhu. *Chin. J. Chem.*, **22**, 142 (2006).
[33] N. Phukan, J.B. Baruah. *RSC Adv.*, **3**, 1151 (2013).
[34] M.J. Plater, M.R. St.J Foreman, R.A. Howie, J.M.S. Skakle, S.A. McWilliam, E. Coronado. *Polyhedron*, **20**, 2293 (2001).
[35] M.D. Allendorf, C.A. Bauer, R.K. Bhakta, R.J.T. Houk. *Chem. Soc. Rev.*, **38**, 1330 (2009).
[36] G. Yu, S. Yin, Y. Liu, Z. Shuai, D. Zhu. *J. Am. Chem. Soc.*, **125**, 14816 (2003).